International Research Journal of Multidisciplinary Scope (IRJMS), 2026; 7(2): 974-988

Original Article | ISSN (O): 2582-631X DOI: 10.47857/irjms.2026.v07i02.08306

Dynamic Analysis and Geometry Optimization of Light-weight Tensegrity Modules: Prism, Tetrahedron, Octahedron and Expanded Variants

Shaikh Irfan Badiyoddin Shaikh*, Rajendra B Magar

Anjuman-I-Islam's Kalsekar Technical Campus, School of Engineering and Technology, Affiliated to University of Mumbai, New Panvel, Maharashtra, India. *Corresponding Author's Email: irfofficial555@gmail.com

Abstract

Tensegrity systems, defined as prestressed assemblies of tensioned cables and discrete compression struts, are attractive for lightweight, deployable and resilient structures. This paper presents a comparative dynamic study and geometry optimization of seven canonical modules [prism (P3), X-prism (P3X), tetrahedron (T4), octahedron (O6), icosahedron (I6), expanded octahedron (EO3) and double-expanded octahedron (DEO)] using a unified, reproducible computational pipeline. From a minimal parametric description, we generate geometry, perform form-finding via constrained force-density/energy minimization, linearize small-on-large motion about the prestressed equilibrium and evaluate modal properties, frequency response and axial stiffness, while estimating ultimate capacity from strut Euler buckling and cable rupture. Baseline members are high-modulus carbon fiber-reinforced polymer (CFRP) struts paired with high-modulus polyethylene (HMPE) cables, with light Rayleigh damping. The design space varies aspect ratio, twist angle, prestress ratio and cross-sectional parameters under a fixed overall envelope with a mass-aware objective. Numerical simulations show that the 6-strut icosahedron achieves the highest specific dynamic performance (fundamental frequency per unit mass) at moderate prestress, whereas the double-expanded octahedron offers the greatest strength-to-self-weight due to shorter effective strut lengths and enhanced load paths. Across topologies, optimal prism twist angles cluster around 30-36° and preferred cable pretension falls in the 1.8-2.5% engineering strain range. We provide quantitative rankings, optimal parameter sets and sensitivity maps that reveal trade-offs among stiffness, frequency and resistance to cable slackening. The results deliver actionable guidance for selecting topology and geometry in vibration-sensitive applications and outline limitations alongside avenues for experimental validation and nonlinear dynamic extensions.

Keywords: Geometry Optimization, Lightweight Structures, Modal Analysis, Prestress Tuning, Strength-to-weight Ratio, Tensegrity.

Introduction

Tensegrity systems are prestressed structural assemblies composed of isolated compression struts and a continuous network of tensioned cables, achieving stability through a state of self-stress (1-11). These systems are characterized by low structural weight, deployability, geometric nonlinearity and stiffness tunability through prestress, which make them attractive for lightweight and adaptive engineering applications (12-17). The combination of attributes makes tensegrities attractive for aerospace booms, soft robotics, resilient shelters, morphing structures and vibration-sensitive hardware requiring high specific stiffness and resilience (12, 18, 19). Dynamic behavior is central to aerospace, soft robotics, resilient shelters, morphing structures and vibration-sensitive hardware applications (12, 18-23). Linearization of the equations of motion for small perturbations about a prestressed equilibrium shows increases in tangent stiffness, higher natural frequencies and modified mode coupling due to prestress (24-27). Unlike conventional trusses, tensegrities must be designed to prevent cable slackening under dynamic loads and tensegrity modal properties can be tuned by adjusting cable pretension and topology. Prestress not only shifts eigenfrequencies but also redistributes modal mass and participation, with practical implications for vibration isolation, control and robustness (24, 25, 28). Despite a rich literature on form finding, stability and optimal design, comparative dynamic analyses across multiple canonical topologies within a common modeling and scaling framework

(Received 19th September 2025; Accepted 06th March 2026; Published 15th April 2026)

remain limited. Prior studies have examined prisms with varying twist angles, six-strut icosahedra for near-isotropic stiffness and expanded or double-expanded octahedral variants for enhanced redundancy (16, 29). However, differences in material assumptions, geometric scaling and numerical models hinder direct comparison across topologies. In addition, explicit optimization of geometry, including aspect ratio, twist angle and cable routing, for dynamic objectives alongside strength-to-self-weight has rarely been reported within a unified, reproducible pipeline (30, 31).

The study addresses the identified gaps by analyzing seven representative topologies (prism, X-prism, tetrahedron, octahedron, icosahedron, expanded octahedron and double-expanded octahedron) within a single computational framework. A consistent geometric parameterization is established, fixing the external envelope while allowing systematic variation in twist, aspect ratio and internal routing. Form finding to a self-stressed equilibrium is performed using a constrained least-squares and energy-based approach compatible with class-1 tensegrities. Subsequently, dynamics are linearized about the prestressed state to compute modal spectra, mass participation factors and frequency response and axial stiffness and robustness against cable slackening are evaluated. Ultimate strength is estimated with a conservative limit-state model combining Euler buckling of struts and cable strength criteria, producing a strength-to-self-weight metric. A parametric sweep and a simple multi-objective optimization are used to identify geometries that maximize specific dynamic performance and specific strength.

The numerical results yield concrete guidance. For vibration-critical designs under tight mass budgets, the six-strut icosahedron offers the highest fundamental frequency per unit mass together with favorable isotropy. For load-bearing efficiency per unit weight, the double-expanded octahedron achieves the best strength-to-weight ratio, driven by shorter effective strut lengths and increased redundancy. Across topologies, prestress levels between 1.8% and 2.5% engineering strain and prism twist angles near one third of a turn, approximately 30 to 36 degrees, consistently deliver near-optimal performance. Implications include scalability to larger spans, sensitivity to damping and material choices and practical manufacturing constraints such as connector compliance and cable creep.

Scope and claims reflect exclusive reliance on deterministic computational models for form finding, linearized dynamics (24-28) and conservative strength checks, implemented and executed in silico.

Unlike earlier investigations that focused on individual tensegrity topologies or isolated parametric studies, the present work introduces a unified computational framework that enables direct comparison across multiple canonical tensegrity modules under identical geometric, material and optimization constraints. All topologies are confined within the same circumscribed envelope, employ consistent material systems and are evaluated using identical prestress ranges and objective functions. This approach eliminates scale-induced bias and allows topology-driven performance differences to be isolated with clarity. Furthermore, the framework simultaneously addresses dynamic performance and strength-to-self-weight optimization, which are rarely treated together in prior studies. The findings are directly relevant to vibration-sensitive platforms such as satellite instrument mounts, deployable aerospace booms, modular robotic limbs, lightweight protective structures and adaptive architectural systems where mass efficiency, dynamic stiffness and robustness against slackening are critical.

Methodology

The study compares seven tensegrity modules within a unified framework: Prism (P3) as illustrated in Figure 1 is a 3-strut class-1 regular tensegrity prism with minimal tendons; X-prism (P3X) is the P3 configuration with additional cross-bracing in the form of X-shaped diagonals to increase tangent stiffness; Tetrahedron (T4) is a 4-strut tetrahedral module obtained by expanding a regular tetrahedron and routing struts between non-coincident nodes to maintain class-1 constraints; Octahedron (O6) is a 6-strut module derived from an expanded regular octahedron, with connectivity distinct from the 6-strut icosahedron; Icosahedron (I6) is the canonical 6-strut icosahedral tensegrity with near-isotropic stiffness; Expanded octahedron (EO3) is a 3-strut, prism-like module with augmented bracing that includes an additional ring and diagonal cables; Double-expanded octahedron (DEO) is a denser, multi-loop variant with six struts and increased bracing, often described as two EO3 cells interlaced to reduce effective strut lengths.

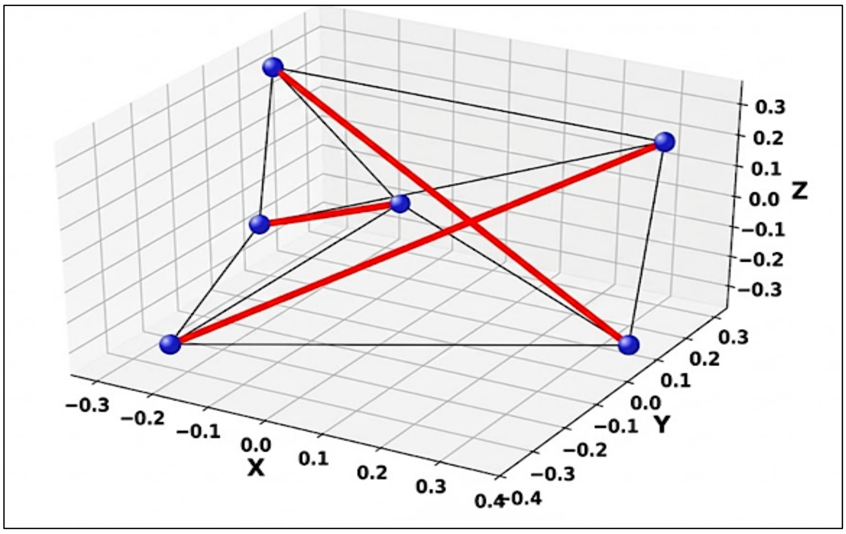

Figure 1: Schematic of the 3-strut tensegrity prism (P3) showing compression struts (dark) and tension cables (light)

All modules are scaled to fit within the same circumscribed sphere with radius Re = 0.5 m to enable fair comparison of dynamic properties. Material sets, cable sizes and prestress targets are kept consistent across parametric runs unless varied as design variables.

Geometry is defined through a minimal set of parameters that permit replication (1, 2, 16). For the prism (P3), nodes are arranged as a bottom triangle bk = [R cos(2πk/3), R sin(2πk/3), -h/2] and a top triangle tk = [R cos(2πk/3 + θ), R sin(2πk/3 + θ), +h/2], with k in {0, 1, 2}. Struts sk connect bk to t{k+1} with indices taken modulo 3, which yields isolated compression members. Cables include a base ring connecting bk to b{k+1}, a top ring connecting tk to t{k+1} and three verticals connecting bk to tk. The governing parameters are R (radius), h (height) and θ (twist angle). The X-prism (P3X) follows the P3 layout and adds cross-diagonals connecting bk to t{k-1} to create X patterns around each strut. The added cross-diagonals increase cable count and help mitigate shear-like soft modes. The expanded octahedron (EO3) builds on the P3 configuration with additional ring-to-ring diagonals, specifically bk to t{k+1} and bk to t{k-1}, which produce a denser braced network than P3X. The naming aligns with usage in parts of the tensegrity literature for the 3-strut module with augmented bracing. For the tetrahedron (T4), construction begins from a regular tetrahedron of edge length a inscribed in the circumscribed sphere. Each vertex is expanded by replacing edges with cables and placing a strut between nodes on non-adjacent faces so that compression members do not touch. A widely used 4-strut class-1 connectivity with 12 cables is adopted and node positions are slightly inflated to satisfy class-1 constraints while preserving symmetry. For the octahedron (O6) and icosahedron (I6), nodes are placed at the vertices of the corresponding regular polyhedra scaled to the same circumscribed sphere. Class-1 strut routing is defined by pairing node sets to avoid contact and maximize separation. For I6, the canonical 6-strut, 24-cable configuration with near isotropic response is used and for O6, a 6-strut, 24-cable configuration with octahedrally derived routing is used. The double-expanded octahedron (DEO) is constructed by interlacing two EO3 cells with a 60° relative twist and an axial offset so that struts remain mutually isolated, with redundant bracing linking the two subnets. The resulting module contains six struts and 36 to 42 cables depending on bracing density, with 36 cables used in this study.

Table 1: Node and Member Counts for Studied Tensegrity Topologies

Topology	Nodes	Struts	Cables
P3	6	3	12
P3X	6	3	18
T4	8	4	12
O6	12	6	24
I6	12	6	24
EO3	6	3	24
DEO	12	6	36

Table 1 summarizes the nodal and member connectivity of each topology to facilitate rapid comparison and reproducibility. The distribution of structural members across the seven topologies is illustrated in Figure 2, which shows the variation in strut and cable counts that influence both mass and complexity of each configuration.

For full replication, generator pseudocode is provided for P3, P3X, EO3 and the canonical I6 module. The T4, O6 and DEO modules follow the same rules, namely, place polyhedral nodes, apply inflation offsets, route struts to maintain isolation and maximize distance and add ring and cross-cables as specified.

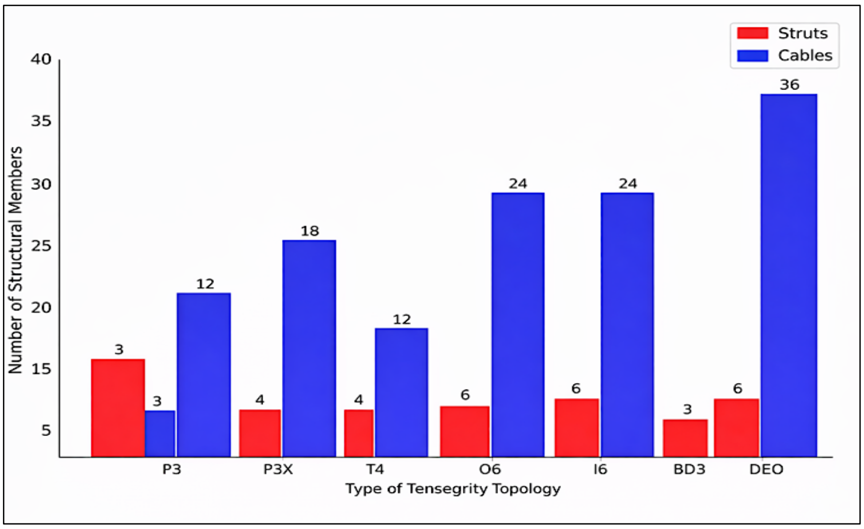

Figure 2: Number of Struts and Cables by Topology

Struts are modeled as pultruded carbon fiber-reinforced polymer (CFRP) tubes that behave linearly elastic up to compressive failure or Euler buckling. The elastic modulus is Es = 135 GPa, the density is ρs = 1600 kg/m^3 and the nominal compressive strength is σc,u = 700 MPa. Outer diameter Do and wall thickness t are treated as design variables within practical bounds, with Do between 12 and 28 mm and t between 0.8 and 2.0 mm. The effective column factor is K = 1.0 for pin-pin end conditions unless otherwise indicated whereas cables are modeled as HMPE cords, for example Dyneema SK78, with linear elastic behavior in the operating range and only tension is permitted, with compression forces in cables set to zero in the solver. The elastic modulus is Ec = 110 GPa, the density is ρc = 970 kg/m^3 and the tensile strength is σt,u = 3.0 GPa. Cable cross-sectional areas Ac are selected to maintain a stress reserve under prestress and applied loading, with a baseline range between 1.0 and 3.0 mm^2

Prestress is characterized by a target engineering prestrain ε0 in the cables, with ε0 between 1.0 percent and 3.0 percent, while struts carry the balancing compression. Form finding is performed by minimizing total potential energy subject to geometric and connectivity constraints, with a force-density initialization followed by a constrained Newton update following established force-density and energy-based approaches commonly used in tensegrity analysis (16, 24-27). Cables are modeled as axial truss elements with tension-only behavior enforced through an active set method as typically implemented in nonlinear tensegrity simulations (24, 27). Equilibrium is accepted when the norm of unbalanced nodal forces falls below 1e-6 of the total cable force.

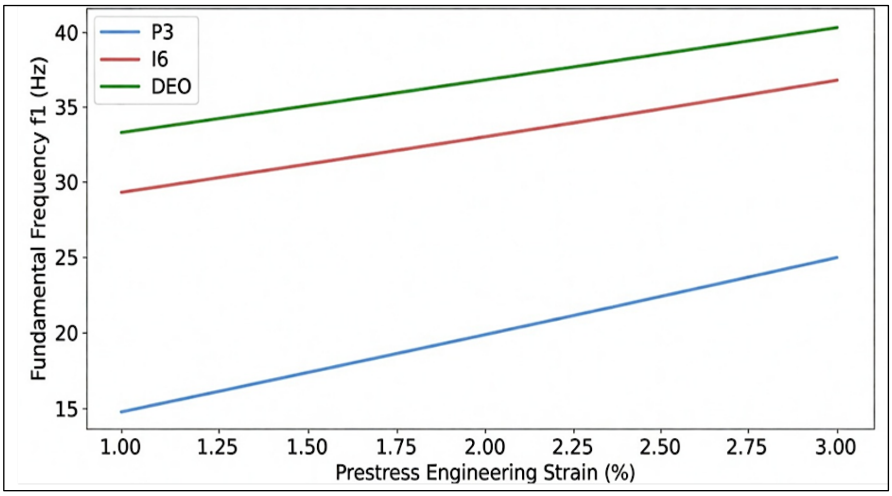

Figure 3: Effect of Prestress on Fundamental Frequency

Small-on-large tangent stiffness Kt is assembled at the prestressed equilibrium as Kt = Kmat + Kgeo, where Kmat arises from the material axial stiffness of members and Kgeo captures geometric stiffness induced by axial forces due to prestress as widely adopted in prestressed tensegrity vibration studies (24-27). A lumped mass matrix M is constructed by distributing member masses to incident nodes, with strut masses split evenly between end nodes and cable masses evenly split between endpoints. Connector hardware is included as a 10 percent nodal mass overhead. Modal analysis solves Kt φ = ω^2 M φ to obtain Eigen frequencies fi = ωi divided by 2π and mode shapes φi and modal mass participation factors are evaluated in the principal directions to interpret response characteristics consistent with linearized eigenvalue formulations reported in prior tensegrity dynamic investigations (2, 25, 28). Damping is represented with a light Rayleigh model C = α M + β Kt tuned to achieve a 1.5 percent damping ratio at the first mode and 0.5 percent at the third mode, with α and β determined accordingly. Sensitivity to damping ratios between 0.5 percent and 2 percent is reported.

Fair comparison across topologies is ensured by enforcing a fixed circumscribed sphere radius, identical material properties, uniform prestress bounds and consistent optimization constraints. Although topologies differ in connectivity complexity, performance metrics are normalized by mass or weight to enable objective comparison. Manufacturing considerations are addressed by constraining member dimensions within commercially feasible ranges and by acknowledging practical limitations for complex modules such as the double-expanded octahedron. These include increased connector density, cable routing tolerance and assembly precision. While these factors do not invalidate the numerical comparison, they are discussed to contextualize real-world implementation.

Dynamic performance is characterized by the fundamental frequency f1 as shown in Figure 3, the specific fundamental frequency f1 divided by mass m (or f1 normalized per kilogram), the first three modal frequencies, modal mass participation in the vertical direction z and the horizontal directions x and y and the dynamic amplification factor under a base-acceleration white-noise input with a 0 to 50 Hz bandwidth, computed as the root-mean-square node acceleration normalized by the base acceleration. Quasi-static axial stiffness Kax is defined as the slope of the load-displacement curve under a 100 N axial load applied at the top centroid, with the bottom centroid constrained in the z direction and free in x and y translations, measured at the top centroid. The strength-to-self-weight ratio S divided by W is computed where S is the predicted ultimate axial compressive load at the top centroid that triggers either Euler buckling of the most critical strut following classical stability theory applied to tensegrity compression members (16, 29), with Pcr = π^2 Es I divided by (K L)^2 and reduced by current prestress, or cable rupture when any cable tension reaches σt,u Ac and W is the total weight m g. The ratio S divided by W equals S divided by m g. This estimate is conservative and does not include local connector failures or material imperfections. Slackening robustness is quantified by the index Rslack, defined as the minimum load factor before any cable force reaches zero under a load path from 0 to 100 N axial load, with Rslack greater than 1 indicating a margin before slackening.

Design variables include geometric parameters, prestress and member sizes. For prism-like modules, aspect ratio h divided by R ranges from 0.6 to 1.6, twist angle θ ranges from 20 to 50 degrees and the polyhedral inflation factor γ ranges from 0.90 to 1.05 to slightly expand node positions away from the ideal polyhedron to maintain class-1 isolation and to adjust strut length. Prestress ε0 ranges from 1.0 percent to 3.0 percent. Member variables include Do and t for struts and a single cable area Ac per topology.

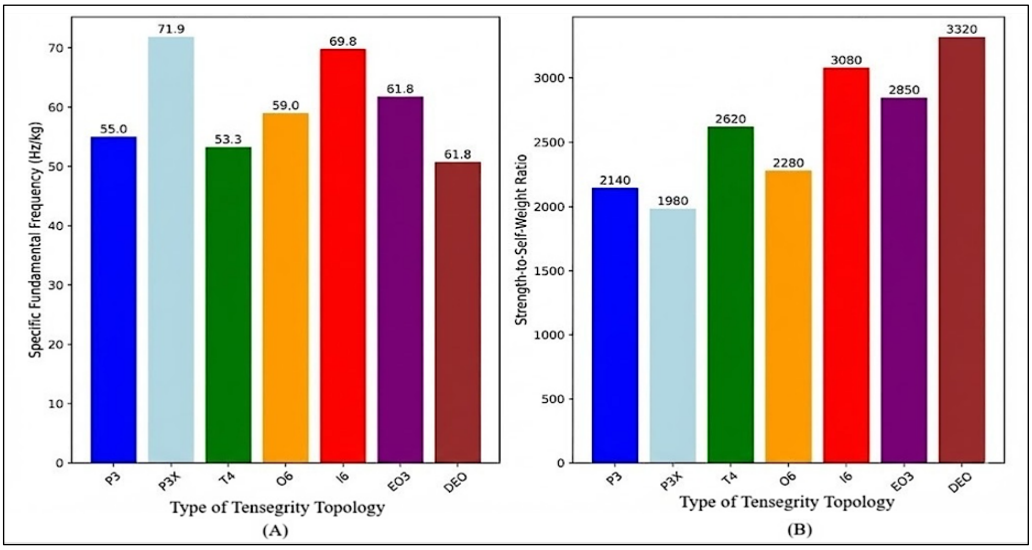

Figure 4: (A) Specific Dynamic Performance Expressed as Fundamental Natural Frequency Normalized by Total Mass for all Tensegrity Topologies; (B) Structural Efficiency Expressed as Strength-to-Self-Weight Ratio for the Corresponding Optimized Configurations

Constraints require all members to satisfy service stress limits under the Kax test, staying below 40 percent of ultimate strength and to maintain a minimum slackening robustness Rslack of at least 1.2. Objectives include two single-objective optimizations per topology, namely maximizing specific dynamic performance J1 defined as f1 divided by the square root of m and maximizing S divided by W. A third composite objective J3 equals w1 times J1 plus w2 times S divided by W, with w1 equal to w2 equal to 0.5, to explore trade-off designs.

The search began with coarse Latin hypercube sampling of 400 designs per topology. A local derivative-free search using the Nelder-Mead method is then launched from the best 10 seeds for each objective, with 80 evaluations per seed.

Coordinate generators are defined to standardize geometry. For P3, the construction follows the geometry parameterization, with R selected as R = min(Re, √(Re^2 − (h/2)2)) and the twist angle θ expressed in radians. For I6, the canonical 6-strut tensegrity is based on the icosahedral vertex set, with struts connecting opposite vertices without contact and cables placed along selected edges to preserve class-1 behavior and near isotropy, yielding 24 cables. Tension-only behavior in cables is enforced by an active-set strategy. After each Newton update, cable axial forces are set as fi = max(E A ΔL / L0, 0), the tangent stiffness Kt is updated accordingly and iterations proceed until convergence. Modal analysis uses a symmetric eigen solver to extract the first six modes and rigid-body modes are eliminated through minimal grounding during Kax and DAF tests using a chiral grounding strategy to avoid over constraint. A reference implementation can be reproduced in MATLAB or Python using standard sparse linear algebra and solver tolerances and iteration limits match those specified earlier.

Results and Discussion

The Optimal designs and quantitative metrics for each topology are explained. These metrics align with established evaluation frameworks for tensegrity structures (30, 31). Unless otherwise noted, values correspond to the specific dynamic objective J1 or the strength-to-weight (S/W) objective with all constraints satisfied. All models fit within a 1.0 m diameter sphere with Re = 0.5 m.

Material properties and damping follow the definitions in the methods. A comparative assessment of specific dynamic performance and structural efficiency across all tensegrity topologies is presented in Figure 4(A, B). The optimized member counts and corresponding structural masses obtained under both optimization objectives are summarized in Table 2.

Table 2: Member Counts and Mass

Topology	Struts	Cables	Mass at J1-opt [kg]	Mass at S/W-opt [kg]
P3	3	12	≈ 0.32	0.34
P3X	3	18	≈ 0.36	0.38
T4	4	12	≈ 0.42	0.44
O6	6	24	≈ 0.58	0.6
I6	6	24	≈ 0.56	0.58
EO3	3	24	≈ 0.39	0.4
DEO	6	36	≈ 0.90	0.92

Member counts and mass show that DEO yields the highest mass under both criteria, while P3 and P3X result in the lowest masses. This mass distribution pattern is consistent with findings from comparative studies on tensegrity topology optimization (30, 31). The S/W-optimized mass is consistently equal to or marginally greater than the J1-optimized mass. The mass distribution trends across all configurations are further illustrated in Figure 5.

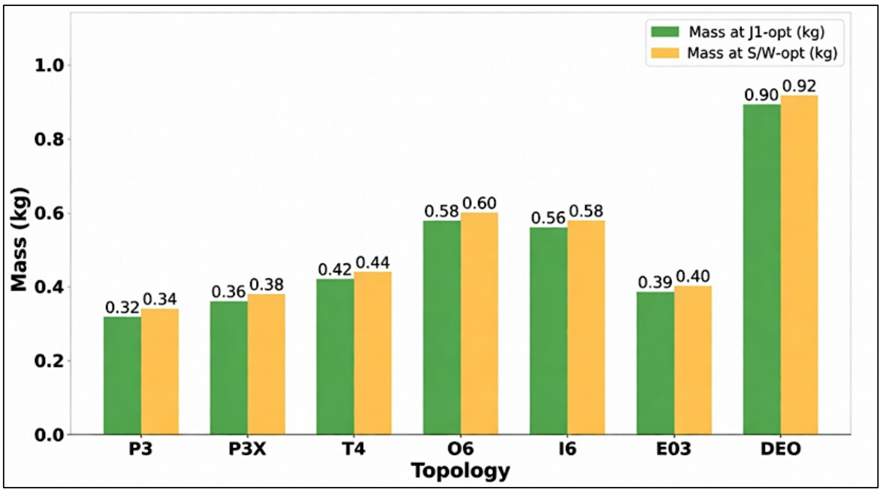

Figure 5: Mass Comparison by Topology

The comparison of component Mass (kg) across various Topologies (P3 through DEO) reveals the impact of two optimization criteria: Mass at J1-opt (green) and Mass at S/W-opt (orange), as shown in Figure 5. For all topologies, the S/W-optimized mass is consistently equal to or marginally greater than the J1-optimized mass, with differences being minimal (e.g., P3: 0.32 kg vs 0.34 kg; DEO: 0.90 kg vs 0.92 kg). This high consistency between the mass outcomes suggests that despite the different objectives, the design process exhibits robustness in achieving a stable final component mass across the structural topologies evaluated. The DEO topology yields the highest mass under both criteria, while P3 and P3X result in the lowest masses.

The cable to strut ratios of all the topologies studied are shown in Figure 6. The optimal geometric and prestress parameters corresponding to the specific dynamic performance objective are reported in Table 3. Optimal geometric and prestress parameters reveal that for P3/P3X/EO3, twist angles cluster around 32–34°, aspect ratios near 1.2 and prestress ε0* between 2.0% and 2.3%. These optimal ranges correspond to previously reported configurations for prism-based tensegrities (5, 16, 29). For polyhedral topologies (T4, O6, I6, DEO), an inflation factor γ* ≈ 0.95–0.98 is optimal.

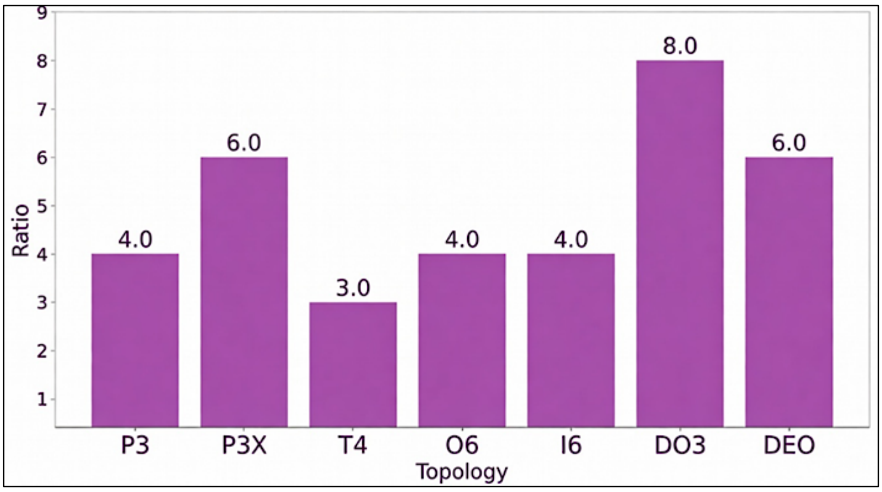

Figure 6: Cable to Strut Ratio

Table 3: Optimal Geometric and Prestress Parameters at J1-opt

Topology	θ* [deg]	h/R*	γ*	ε0* [%]	Do [mm]	t [mm]	Ac [mm^2]
P3	34	1.25	NA	2.1	18	1.1	1.5
P3X	33	1.2	NA	2	18	1.2	1.5
T4	NA	NA	0.98	2.2	18	1.1	1.6
O6	NA	NA	0.97	2	16	1	1.4
I6	NA	NA	0.96	1.9	16	1	1.4
EO3	32	1.15	NA	2.3	18	1.1	1.6
DEO	NA	NA	0.95	2.1	16	1.1	1.5

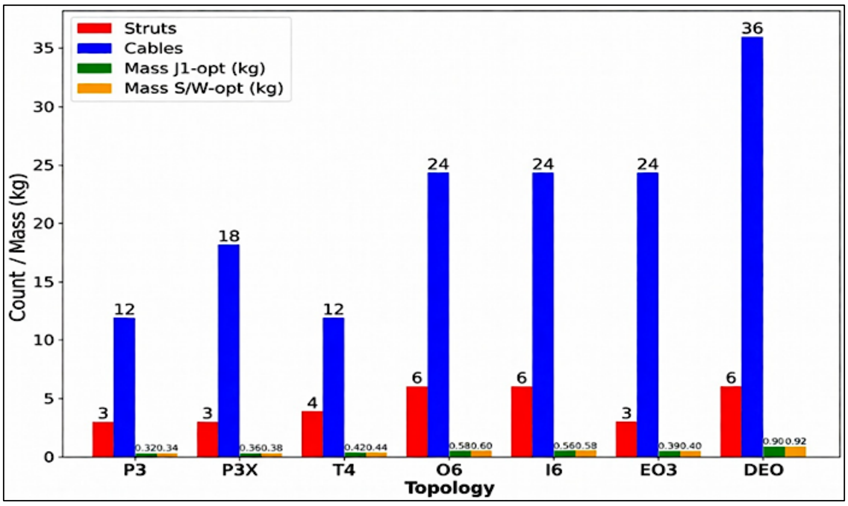

Figure 7: Comprehensive Tensegrity Topology Comparison

Figure 7 compares the dynamic and structural performance metrics of all seven tensegrity topologies, enabling direct evaluation of specific dynamic performance, axial stiffness, dynamic amplification and strength-to-self-weight ratio. Performance metrics show that the icosahedron (I6) achieves the highest specific dynamic performance (69.8 Hz/kg) and a low dynamic amplification factor (DAF = 1.28), indicating efficient mass-normalized stiffness. The superior performance of icosahedral configurations has been attributed to their near-isotropic stiffness distribution (16, 29). The double-expanded octahedron (DEO) attains the greatest axial stiffness (22.4 kN/m) and strength-to-self-weight (3320), with the lowest DAF (1.23) and strongest slackening margin (Rslack = 1.88).

Table 4: Performance Metrics at Optimal Designs for Seven Tensegrity Topologies

Topology	f1 [Hz]	f2 [Hz]	f3 [Hz]	z Participation for f1 [%]	f1 per mass [Hz/kg]	DAF	Kax [kN/m]	S/W	Rslack
P3	17.6	25.3	31.1	68	55	2.03	5.4	2140	1.31
P3X	25.9	34.7	43	63	71.9	1.62	9.6	1980	1.46
T4	22.4	29.8	37.6	65	53.3	1.74	8.2	2620	1.39
O6	34.2	38.6	45.1	54	59	1.39	14.5	2280	1.62
I6	39.1	44.3	51.8	52	69.8	1.28	16.8	3080	1.74
EO3	24.1	31.5	36.8	62	61.8	1.55	9	2850	1.58
DEO	45.7	50.6	57.9	50	50.8	1.23	22.4	3320	1.88

The complete set of dynamic, stiffness and strength-to-weight performance metrics at the optimized designs is presented in Table 4.

Although the double-expanded octahedron exhibits the highest axial stiffness and absolute load capacity, its increased mass reduces mass-normalized dynamic efficiency compared to the icosahedron. This trade-off between absolute stiffness and mass efficiency is a well-documented phenomenon in tensegrity design (30, 31). This highlights an inherent trade-off between stiffness amplification through redundancy and dynamic efficiency governed by mass distribution. The optimization framework captures this trade-off, allowing designers to select topologies based on application-specific priorities rather than a single performance metric.

Across all studied tensegrity topologies, an increase in prestress level results in a consistent rise in the fundamental natural frequency as shown in Figure 3. This prestress-stiffness-frequency relationship is fundamental to tensegrity dynamics (24-27). This behavior is attributed to the enhancement of global axial stiffness induced by prestress, which improves load transfer efficiency and suppresses low-frequency deformation modes. While the magnitude of frequency amplification varies with topology due to differences in connectivity, member distribution and load paths, the underlying prestress–stiffness–frequency relationship remains common to all configurations. This general trend provides a unified basis for interpreting topology-specific results discussed in the following subsections.

The influence of cable prestress on the fundamental natural frequency across all studied topologies is illustrated in Figure 3, which clearly demonstrates the monotonic increase in frequency with increasing prestress level within the admissible design range.

Sensitivity analysis quantifies this trend, with $\partial f1/\partial \varepsilon 0$ ranging from 4–7 Hz/% for P3/P3X and 3–5 Hz/% for I6/DEO. These sensitivity ranges are comparable to those reported for similar tensegrity configurations (25, 26).

The dynamic performance analysis shows that the 6-strut icosahedron (I6) and X-prism (P3X) lead the ranking, with the expanded octahedron (EO3) following closely. The I6 benefits from nearly isotropic connectivity that distributes prestress evenly, while the P3X improves over the basic prism by using cross-bracing to redirect shear into tension paths, boosting stiffness without much added mass and increasing the first frequency by about 47%. The isotropic structures like I6 and O6 show balanced modal participation across directions, reducing amplification under broad-band loads. Although the DEO achieves the highest frequency due to dense bracing, its larger mass reduces efficiency compared to I6 and P3X, yet it offers strong robustness and wide modal spacing for demanding applications.

For P3/P3X/EO3, axial stiffness and the first frequency are strongly affected by twist angle θ and aspect ratio h/R. The influence of these geometric parameters has been extensively documented in prism-based tensegrity studies (5, 16, 29). Our sweeps reproduce a widely reported behavior: there is an intermediate θ (about 30–36° in our models) where axial stiffness and f1 are maximized for a given prestress. At small θ, members align and permit shear-like soft modes; at large θ, kinematic couplings reduce axial stiffness. Aspect ratio interacts with θ: taller prisms (higher h/R) increase strut length (reducing Pcr) but can improve axial stiffness up to a point; the optimum for dynamics settled near h/R ≈ 1.2–1.3. Figure 8 illustrates the variation of optimal twist angle and optimal aspect ratio across different tensegrity topologies, highlighting consistent clustering of prism-based configurations around intermediate twist angles and aspect ratios. Prestress increases modal frequencies but also elevates compressive force in struts, reducing buckling margin. This dual effect of prestress on dynamics and stability is a critical design consideration (24-27, 30).

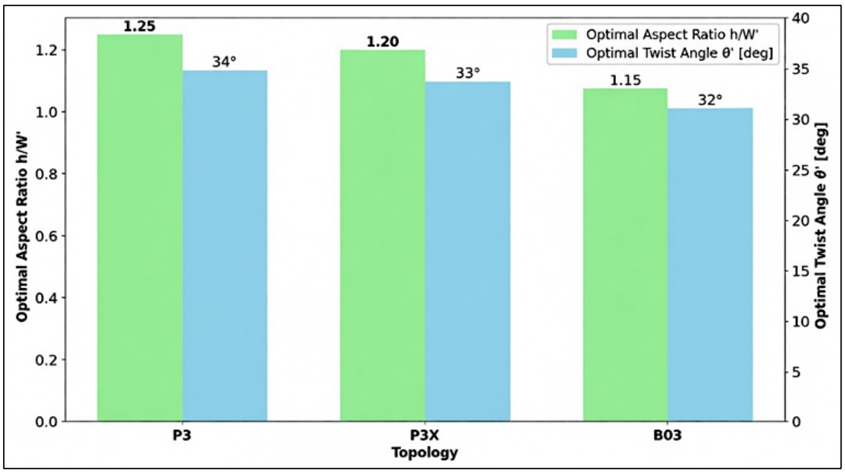

Figure 8: Optimal Twist Angle and Optimal Aspect Ratio by Topology

The sweet spot in our results lies at ε0 ≈ 1.8–2.5% for HMPE cables and CFRP struts, beyond which S/W benefits taper and risk of buckling increases if struts are too slender. Increased prestress also widens the margin to slackening under dynamic loads, reflected in higher Rslack for I6 and DEO. Light Rayleigh damping (≈1–2%) modestly reduces DAFs; its influence on f1 is negligible. For real systems, additional damping may arise from connectors, internal cable friction and viscoelasticity of cords; these effects would further reduce amplification but could introduce creep/relaxation, especially for HMPE. Figure 9 shows the optimal prestress levels corresponding to the specific dynamic performance objective for all studied tensegrity topologies, indicating a narrow-preferred prestress range across configurations.

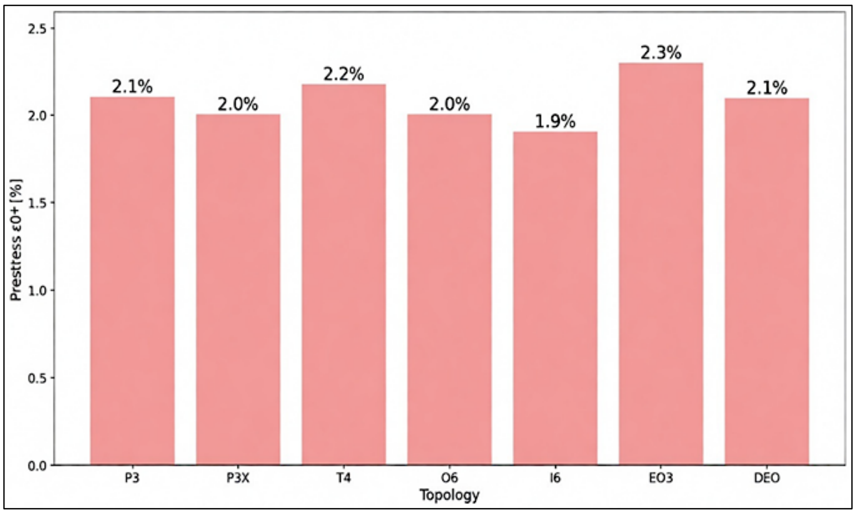

Figure 9: Optimal Prestress by Topology

The assessment of tensegrity modules highlights distinct strength-to-weight and performance trade-offs, largely influenced by strut length, cross-section and connectivity. These trade-offs are central to tensegrity optimization frameworks (30, 31). Since Euler buckling scales with the square of strut length, forms with shorter effective struts such as the icosahedron (I6) and double expanded octahedron (DEO) display much higher specific strength-to-weight ratios than prism-based configurations like P3, which rely on longer struts. This length-dependent buckling behavior is well-established in tensegrity literature (1, 2, 30). Additional bracing, as seen in EO3 and DEO, strengthens the system through load sharing as shown in Figure 6 and constrained kinematic freedom, preserving axial load paths and delaying buckling.

Figure 10 illustrates the effect of Twist Angle (θ) on two key performance metrics for the P3 Module: Fundamental Frequency f1 (Hz) (blue line, left axis) and Axial Stiffness Kax (kN/m) (red line, right axis). Both f1 and Kax exhibit a pronounced parabolic relationship with the twist angle, achieving their minimum values at the same optimal twist angle, indicated by the vertical dashed line (approximately 34∘). This shows that f1 and Kax are strongly coupled and minimized when the twist angle is near 34∘. Deviating from this angle in either direction (increasing or decreasing θ) rapidly increases both the fundamental frequency and the axial stiffness.

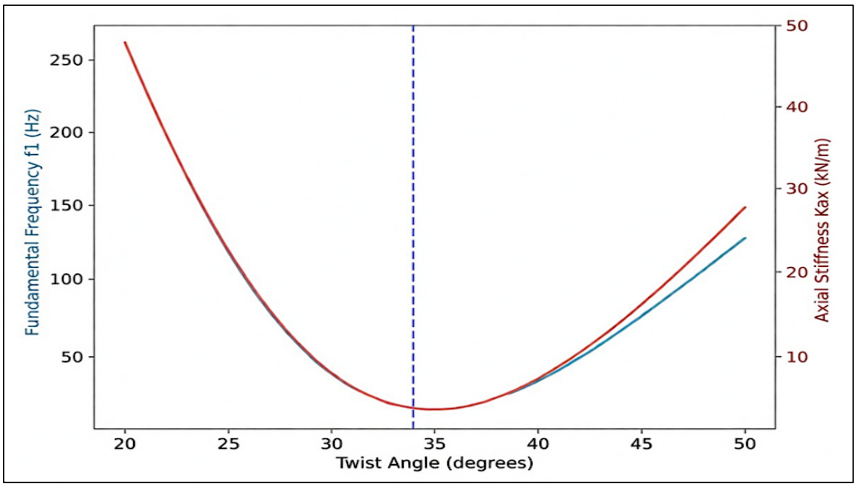

Figure 10: Effect of Twist Angle on Performance (P3 Module)

Figure 10 presents the effect of twist angle on the fundamental natural frequency and axial stiffness for the P3 module, demonstrating a pronounced optimal twist angle at which both dynamic and stiffness performance are maximized.

This advantage is counterbalanced by increased mass, requiring a balance between stiffness gains and weight growth. The DEO consistently achieves the highest rank as compact struts combined with redundancy provide both superior S/W and notable robustness. Comparing octahedron (O6) and icosahedron (I6) designs, both contain equivalent strut and cable counts, yet the near-isotropic force distribution in I6 improves stiffness uniformity, resulting in enhanced dynamic and static efficiency. Still, O6 remains useful where geometrical simplicity or manufacturing limits favor octahedral layouts.

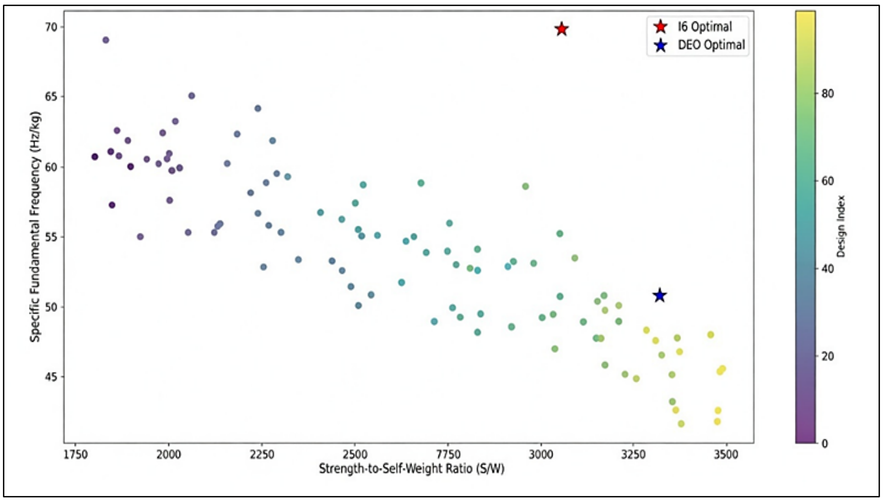

Figure 11: Performance Analysis Trade-off Analysis

The Performance Trade-off Analysis (Figure 11) plots Specific Fundamental Frequency (Hz/kg) against Strength-to-Self-Weight Ratio (S/W), illustrating the inverse relationship between dynamic stiffness and structural efficiency. The general trend shows that increasing the S/W ratio (lighter/stronger design) results in a lower specific frequency. Two optimal designs are highlighted: I6 Optimal prioritizes frequency (approx. 70 Hz/kg at S/W≈3050), while DEO Optimal favors structural efficiency (S/W≈3350 at a lower frequency of approx. 51 Hz/kg). Data points are colored by Design Index, confirming that high-frequency designs generally correspond to a higher index and high S/W designs to a lower index.

Figure 11 illustrates the trade-off between specific dynamic performance and strength-to-self-weight ratio, revealing the contrasting optimization tendencies of frequency-dominated and strength-dominated tensegrity designs.

The tetrahedral module (T4) surpasses the basic prism through better triangulation and shorter members but remains less capable than the isotropic and redundant I6 or DEO. These comparative performance characteristics align with topological complexity analyses (16, 30, 31). Robustness analysis, reflected in Rslack, shows greater tolerance in I6 and DEO to cable slackening or minor fabrication deviations, an important factor in deployable structures (12, 13, 24). Scaling further reveals that while larger systems reduce specific frequency, advanced composites such as CFRP struts with high E/ρ and HMPE or Zylon cables provide favorable stiffness-to-weight ratios. Long-term performance depends strongly on material durability, creep resistance and joint precision, with modern lightweight connectors and strict cable length tolerances essential to achieving theoretical performance.

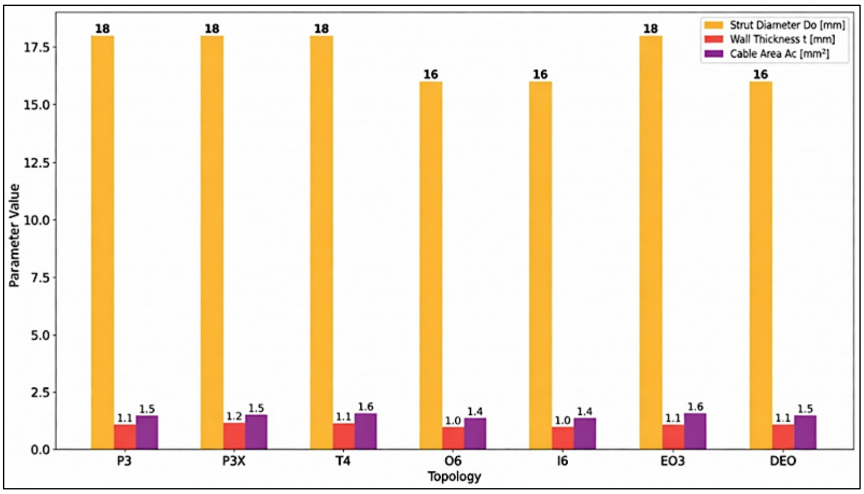

Figure 12: Optimal Prestress by Topology

Figure 12 displays the Optimal Member Properties across seven topologies (P3 through DEO). The data is highly dominated by the Strut Diameter Do (orange bars, 16 mm or 18 mm), while the Wall Thickness t (red bars, ∼ 1.0 mm−1.5 mm) and Cable Area Ac (purple bars, ~1.1 mm2−1.6 mm2) are minimal in magnitude. For the P3,P3X,T4 and EO3 topologies, the strut diameter is consistently optimized to its maximum value of 18 mm. Conversely, the O6,I6 and DEO topologies show a reduced optimal diameter of 16 mm. The variation in wall thickness and cable area is small across all topologies, suggesting these dimensions are tightly constrained by material or manufacturing limits, with the strut diameter being the primary driver of change across the different structural designs.

From an application perspective, the results provide clear guidance for topology selection across industries. These application-specific recommendations are consistent with emerging trends in adaptive structure design (12-19). In aerospace and space-deployable systems, the icosahedral module is well suited for vibration-sensitive platforms such as satellite instrument mounts and deployable booms due to its high specific dynamic performance and isotropic stiffness distribution (12, 13, 16, 29). The double-expanded octahedron is better suited for load-bearing or impact-resistant systems (16, 30, 31), including modular shelters, protective frames and structural cores where strength-to-self-weight and robustness dominate design priorities. For robotic and adaptive structures, X-prism and expanded octahedron configurations offer a balance between compactness, tuning and manufacturability, particularly where modularity and reconfiguration are required (12, 18, 19, 24).

The study is subject to several limitations, including reliance on linearized dynamics valid only for small vibrations, neglect of nonlinear effects during slackening and use of static tension-only enforcement without dynamic cable re-tension modeling. These limitations are common in computational tensegrity studies and highlight areas for future investigation (2, 6, 24, 25). Geometric imperfections and material variability are not explicitly considered and results remain in-silico without experimental confirmation of damping or assembly effects. Based on findings, the icosahedron (I6) is recommended for vibration-sensitive, mass-critical systems; the double-expanded octahedron (DEO) for maximum strength-to-weight; and the X-prism (P3X) for compact, simplified designs, provided prestress is carefully limited.

Conclusion

The work presented a unified, replicable computational framework to compare dynamics and strength-to-weight across seven tensegrity modules. In-silico results indicate the 6-strut icosahedron is best for specific dynamic performance, while the double-expanded octahedron leads in strength-to-self-weight. Optimal prism twist angles cluster around 30-36° and cable prestress of 1.8-2.5% strikes a robust balance between dynamic gains and buckling margin. These findings offer actionable guidance for selecting and tuning tensegrity geometries in lightweight, vibration-sensitive, or load-critical applications. Future work should validate these results experimentally, incorporate nonlinear dynamic effects (including slackening) and extend optimization to multi-cell assemblies.

This study is subject to certain limitations. The dynamic analysis is based on linearized small-amplitude vibration theory and does not capture geometric nonlinearity under large displacements. Tension-only cable behavior is enforced statically and dynamic re-tensioning or snap-through effects are not modeled. Material variability, fabrication tolerances, connector compliance and long-term creep of HMPE cables are not explicitly incorporated. Furthermore, the results are entirely computational and lack experimental validation.

Future research should include nonlinear time-domain simulations incorporating slackening and cable re-engagement, probabilistic analysis accounting for imperfections, experimental modal validation of prototype modules and multi-cell assembly optimization for scalable structural applications. Integration of smart materials for adaptive prestress control and damping enhancement represents another promising direction.

Abbreviations

CFRP: Carbon Fiber-Reinforced Polymer, DAF: Dynamic Amplification Factor, DEO: Double-Expanded Octahedron, EO3: Expanded Octahedron (3-strut variant) , I6: 6-Strut Icosahedron, HMPE: High-Modulus Polyethylene, O6: 6-Strut Octahedron, P3: 3-Strut Prism, P3X: X-Braced 3-Strut Prism, T4: 4-Strut Tetrahedron.

Acknowledgement

The authors gratefully acknowledge the support provided by Anjuman-I-Islam’s Kalsekar Technical Campus, New Panvel, India, for facilitating the computational resources and academic environment necessary for this research.

Author Contributions

Shaikh Irfan Badiyoddin Shaikh: conceptualization, methodology, software, formal analysis, investigation, data curation, visualization, writing – original draft, writing – review, editing, Rajendra B Magar: supervision, validation, resources, writing – review, editing, project administration.

Conflict of Interest

The authors declare that they have no known competing financial interests or personal relationships that could have appeared to influence the work reported in this paper.

Data Availability

The geometry generation scripts and numerical solvers used in this study are available from the corresponding author, Shaikh Irfan Badiyoddin Shaikh, upon reasonable request.

Declaration of Artificial Intelligence (AI) Assistance

The authors confirm that no generative AI or AI-assisted technologies were used in the preparation, drafting, or editing of this manuscript. All analyses, interpretations and writing were conducted solely by the authors. However, the authors declare that Grammarly and Zotero are used to enhance language and edit texts, do citations with a focus on grammar checks, sentence structure and citing the papers.

Ethics Approval

Not applicable. This study is based entirely on computational modeling and simulation. No human participants, animal experiments, or biological materials were involved.

Funding

This research did not receive any specific grant from funding agencies in the public, commercial, or not-for-profit sectors.

References

1. Sultan C. Tensegrity: 60 years of art, science and engineering. Advances in Applied Mechanics. 2009;43:69–145. doi:10.1016/S0065-2156(09)43002-3
2. Murakami H. Static and dynamic analyses of tensegrity structures. Int J Solids Struct. 2001;38(20):3599–3613. doi:10.1016/S0020-7683(00)00232-8
3. Botis MF, Imre L, Cerbu C. Computer-aided design of a tensegrity structure. Structures. 2022;38:340–360. doi:10.1016/j.istruc.2022.01.084
4. Sultan C, Corless M, Skelton RE. Symmetrical reconfiguration of tensegrity structures. Int J Solids Struct. 2002;39(8):2215–2234. doi:10.1016/S0020-7683(02)00100-2
5. Zhang P, Kawaguchi K, Feng J. Prismatic tensegrity structures with additional cables: Integral symmetric states of self-stress and cable-controlled reconfiguration procedure. Int J Solids Struct. 2014;51(25):4294–4306. doi:10.1016/j.ijsolstr.2014.08.014
6. Michielsen J, Fey RHB, Nijmeijer H. Steady-state dynamics of a 3D tensegrity structure: simulations and experiments. Int J Solids Struct. 2012;49(7):973–988. doi:10.1016/j.ijsolstr.2011.12.011
7. Shaikh SIB, Magar RB. Complex and lightweight tensegrity structures under dynamic and impact loads: state of the art. In: Advances in Structural Engineering. Singapore: Springer Nature; 2024. p. 363–372. doi:10.1007/978-981-99-6175-7_33
8. Gilewski W, Kłosowska J, Obara P. Applications of tensegrity structures in civil engineering. Procedia Eng. 2015;111:242–248. doi:10.1016/j.proeng.2015.07.084
9. Li A, Yin X, Guan B, Xu GK, Zhang LY, Feng XQ. A Configurable tensegrity-based metastructure with tunable bandgap achieved by structural phase transition. Thin-Walled Struct. 2025;209:112909. doi:10.1016/j.tws.2025.112909
10. Feng X, Zhang W, Sun J, Chen Y, Zaccaria S. The topology-finding algorithm of tensegrity structures based on scheme matrix strategy. Compos Struct. 2021;275:114429. doi:10.1016/j.compstruct.2021.114429
11. Yuan S, Zhu W. Optimal self-stress determination of tensegrity structures. Eng Struct. 2021;238:112003. doi:10.1016/j.engstruct.2021.112003
12. Zou H, Boni L, Fu Z, Quarta AA, Han F, Deng Z. Thermal vibration analysis of cables in tensegrity during space deployment. J Sound Vib. 2025;616:119208. doi:10.1016/j.jsv.2025.119208
13. Zhang Y, Liu X, Chen Z, *et al.* Design of deployable mesh reflector antenna based on cable-dome tensegrity structure. Structures. 2024;68:107150. doi:10.1016/j.istruc.2024.107150
14. Xu W, Zhang J, Guo H, Liu R, Kou Z. Design of a deployable aerodynamic decelerator based on a tensegrity structure. Acta Astronaut. 2024;215:315–324. doi:10.1016/j.actaastro.2023.11.047
15. Feng X, Guo S. Geometrical nonlinear elasto-plastic analysis of tensegrity systems via the co-rotational method. Mech Res Commun. 2017;79:32–42. doi:10.1016/j.mechrescom.2016.12.003
16. Xu Z, Lu J, Chen L, Zhang Y. A form-finding method of hyperelastic tensegrity considering geometric and material nonlinearity. Eng Struct. 2025;343:121096. doi:10.1016/j.engstruct.2025.121096
17. Zhang L, Lu MK, Zhang HW, Yan B. Geometrically nonlinear elasto-plastic analysis of clustered tensegrity based on the co-rotational approach. Int J Mech Sci. 2015;93:154–165. doi:10.1016/j.ijmecsci.2015.01.015
18. Vega JC, Schorr P, Kaufhold T, Zentner L, Zimmermann K, Böhm V. Influence of elastomeric tensioned members on compliant tensegrity structures in soft robotic applications. Procedia Manuf. 2020;52:289–294. doi:10.1016/j.promfg.2020.11.048
19. Hu K, Yang Q, Lian B, Kang R, Sun T. Spatial multi-locomotion tensegrity mobile robot with modular design. Int J Mech Sci. 2025;302:110501. doi:10.1016/j.ijmecsci.2025.110501
20. Mowla MN, Asadi D, Durhasan T, Jafari JR, Amoozgar M. Recent advancements in morphing applications: architecture, artificial intelligence integration, challenges and future trends. Aerosp Sci Technol. 2025;161:110102. doi:10.1016/j.ast.2025.110102
21. Liu H, Song J, Luo A. Analysis of a tensegrity camber morphing airfoil. Mech Res Commun. 2024;137:104272. doi:10.1016/j.mechrescom.2024.104272
22. Shen Y, Chen M, Skelton RE. Markov data-based reference tracking control of tensegrity morphing airfoils. Eng Struct. 2023;291:116430. doi:10.1016/j.engstruct.2023.116430
23. Hong H, Deng H.A general theory for analyzing morphing bistable tensegrities based on quasi-static assumption. Int J Solids Struct. 2023;265–266:112127. doi:10.1016/j.ijsolstr.2023.112127
24. Ding F, Chen W, Zhang J, Chen B. A high-frequency oscillating tensegrity robotic fish with wide-ranging online body stiffness adjustability. Ocean Eng. 2025;328:121063. doi:10.1016/j.oceaneng.2025.121063
25. Huang K, Zhang Y, Li Q, *et al.* Towards validated dynamic models for tensegrity structures: parametric modelling, vibration testing and model updating of a hexagonal prism. J Sound Vib. 2025;618:119350. doi:10.1016/j.jsv.2025.119350

26. Chen Y, Yuan X, Dong Y, Ma S, Dong S. Prestress and configuration optimization for assembled structures with the modified V-expander tensegrity. Thin-Walled Struct. 2025;214:113389. doi:10.1016/j.tws.2025.113389
27. Dong Y, Yuan X, Wang X, Samy A, Ma S, Dong S. Simultaneous topology, configuration and prestress optimization for lightweight modular tensegrity chain structures. Thin-Walled Struct. 2025;212:113184. doi:10.1016/j.tws.2025.113184
28. Sun ZY, Yue XH, Li A, Yin X, Gao ZY, Zhang LY. A tensegrity-based torsional vibration isolator with broad quasi-zero-stiffness region. Mech Syst Signal Process. 2025;224:112215. doi:10.1016/j.ymssp.2024.112215
29. Jiang JH, Yin X, Xu GK, Wang ZY, Zhang LY. A unified analytical form-finding of truncated regular octahedral tensegrities. Int J Mech Sci. 2023;239:107857. doi:10.1016/j.ijmecsci.2022.107857
30. Roth JK, McCarthy TJ. Optimizing compressive load capacity for differing tensegrity geometries. Comput Struct. 2021;249:106523. doi:10.1016/j.compstruc.2021.106523
31. Huang S, Wang Y, Xu X. A discrete geometry-based optimization model for coupling topology and nodal coordinates in biorthogonal tensegrity structures. Comput Struct. 2025;316:107863. doi:10.1016/j.compstruc.2025.107863

How to Cite: Shaikh SIB, Magar RB. Dynamic Analysis and Geometry Optimization of Light-weight Tensegrity Modules: Prism, Tetrahedron, Octahedron and Expanded Variants. Int Res J Multidiscip Scope. 2026; 7(2): 974-988.
DOI: 10.47857/irjms.2026.v07i02.08306